REGULAR ARTICLE

Geometry, electronic structure, and magnetic ordering of iron–carbon nanoparticles

M. V. Ryzhkov · B. Delley

Abstract The geometry optimization of Fe_nC_m and $Fe_nC_m^+$ nanoparticles from FeC_4 to Fe_7C_8 was carried out using $DMol^3$ method. The most stable isomers for neutral and charged clusters are found with the use of 'binomial' scheme. For each investigated composition, the value of binding energy per atom for the ground isomer was evaluated as well as the number of configurations with binding energies which are close to that of the ground geometry. In almost all compositions, the isomers with ferromagnetic ordering of spins on Fe atoms are found to have the greater dissociation energy than those with any other spin ordering.

Keywords Fe_nC_m: ground isomers · Relative stability · Magnetic ordering

1 Introduction

Since the discovery of the metallocarbohedrene Ti_8C_{12} in 1992 [1], the molecular systems M_xC_y became the subjects of numerous experimental and theoretical investigations. The electronic structure of nanoparticles containing iron atoms Fe_nC_m is also interesting due to the position of Fe between the early and late transition metals (TM). Theoretical investigations of M_xC_y clusters containing the early (V) and late TM (Ni, Co) were presented in [2–5]. There are two ways to generate small Fe–C clusters. Firstly, such

objects can be produced by grinding of solid-phase carbides. Though the maximum carbon content in all crystalline Fe carbides Fe_xC_y does not exceed 1/3 ($y/x \leq 1/3$) [6], the Fe_nC_m fragments of crystal lattice could be of various stoichiometry when the object dimensions are small (m, $n < 20$). Second way of binary Fe_nC_m clusters generation is the laser vaporization of Fe metal and cooling in acetylene. In experimental work of Pilgrim and Duncan [7], the distribution of cationic $Fe_nC_m^+$ particles had been obtained. According to these results, the first observed cluster has (5,6) composition and small relative abundance. The most abundant $Fe_nC_m^+$ species have (7,8), (8,12), and (12,12) content [7]. Theoretical modeling of iron–carbon clusters also follows two ways: Harris and Dance [8] started from $Fe_{12}C_{12}$ fragment of the cubic crystal lattice and investigated the dissociation series $Fe_{12}C_{12} \rightarrow Fe_2C_{12}$. However, the more popular way to construct the initial configurations for geometry optimization was the use of combinations of iron and carbon dimers or C_n chains or the analogs of known metallocarbohedrenes [9–16].

The serious difficulty in theoretical investigations of various Fe_nC_m clusters is the existence of a large amount of isomers for each composition (n, m) and the absence of a fast scheme for reliable generation of the ground geometrical structure. Usually, the search for stable geometries results in the definition of some part of the possible isomers, the lowest energy configuration is considered as the ground geometry for this Fe_nC_m particle. Earlier in our investigations of electronic structure of small iron–carbon clusters [17, 18], the 'binomial' scheme for the generation of stable isomers was suggested (Fig. 1). From our point of view, this scheme is a reliable way to find all possible geometries for any composition (n, m). The shortcoming of this method is the fast increasing amount of isomers as the number of atoms increases, especially for the cases $n/m \sim 1$

M. V. Ryzhkov (✉)
Institute of Solid State Chemistry, Ural Branch of the Russian Academy of Sciences, 620219 Ekaterinburg, Russian Federation
e-mail: ryz@ihim.uran.ru

B. Delley
Paul Scherrer Institut, WHGA 123, 5232 Villigen PSI, Switzerland
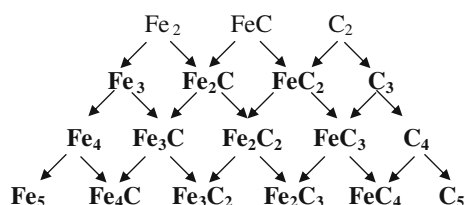
Fig. 1 The scheme for search of the stable structures for Fe_nC_m particles

[18]. However, the analysis of the parentage of the ground configurations for FeC_2, Fe_2C, FeC_3, Fe_3C, Fe_2C_2, and Fe_2C_3 showed that in all cases, the most stable isomer Fe_nC_m was obtained from the most stable configurations of both 'preceding' particles $Fe_{n-1}C_m$ and Fe_nC_{m-1} by the addition of Fe or C atoms, respectively. Thus, to find the ground geometry for any Fe_nC_m cluster, one needs to consider only the ground isomers of all previous compositions.

The aims of the present work are: (1) the search for the probable ground structures of the Fe_nC_m and $Fe_nC_m^+$ clusters for $5 \leq n + m \leq 15$; (2) the evaluation of the trends in binding energy variation along n and m series; (3) the check-up of assumption that ferromagnetic ordering of spin moments on metal sites is preferable for the ground isomers; (4) the comparison of stabilities of the clusters generated by addition of atoms 'one by one' and by grinding of the most stable solid-phase carbide Fe_3C.

2 Objects and methods of calculations

In the present work, the search for Fe_nC_m stable structures followed the 'binomial' scheme, i.e., Fe and C atom approached the known ground isomers of Fe_2C_2, Fe_3C, FeC_3, and Fe_2C_3 [17, 18] from all possible directions. Then, the resulting ground configurations for FeC_4, Fe_2C_4, Fe_3C_2, and Fe_3C_3 served as initial objects for generating the structures of Fe_nC_m particles with greater n and m values. We did not take into account the 'chemical preference' of some directions because when adding the extra atom on all geometrically possible sites for forming a bond, the $DMol^3$ procedure can always 'catch' any nearby configuration with local minimum of energy. The two paths of each cluster generation (Fig. 1) give one a possibility for the verification of the results.

Geometry optimization of Fe_nC_m particles was performed using the $DMol^3$ program [19] in spin-unrestricted approach and with double numerical atomic basis set with d-polarization function for C ('dnd'). The Coulombic potential was computed with the use of model density obtained as decomposition of charge density into multipolar components including those with $l = 3$. The
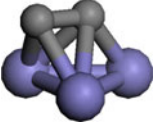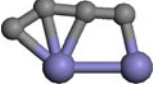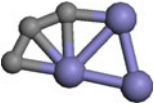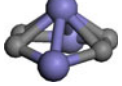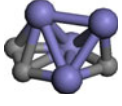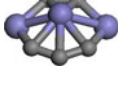
generalized gradient approximation (GGA) in 'PBE' [20] and 'BLYP' [21, 22] forms was used in all calculations. Optimization of the molecular structures was done until change in a value of maximum energy gradients was less than 0.001 atomic units, the global orbital cutoff was 8.0 Å. The thermal smearing of 0.005 was employed to accelerate the convergence of SCF process. However, the thermal smearing could lead to some increase in molecular size and dissociation energies [18]. To confirm that the stationary points correspond to minima, the vibrational frequencies were computed for all isomers obtained. The binding energy of each resulting geometry obtained from different starting configurations can vary within 0.1 eV, mainly for less symmetrical structures.

Since the $DMol^3$ code incorporates only the qualitative schemes of Mulliken [23] and Hirshfeld [24] for the calculation of the effective charges on atoms (Q_{eff}), we also used the Discrete Variational method (DVM) [25, 26]. For each final configuration obtained by $DMol^3$, the DV calculation was carried out, where Q_{eff} is computed as the integral of electron density inside the domain bounded by the points of its minimum [27].
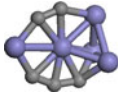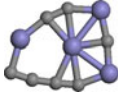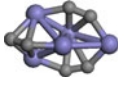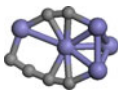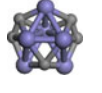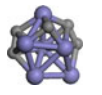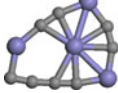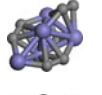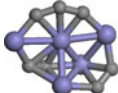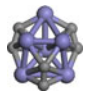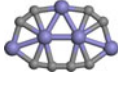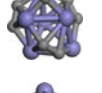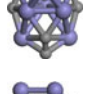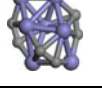
3 Results of geometry optimization

In Table 1, we present the results of our calculations for the neutral Fe_nC_m clusters generated according to 'binomial' scheme. In Appendix, for these most stable isomers, we report their atomic coordinates that could be helpful for the understanding of geometrical structures and could be used in the further theoretical and experimental researches. As can be seen, the 'PBE' functional noticeably overestimates the absolute values of E_b in comparison with the energies obtained using 'BLYP' approach. However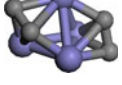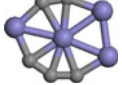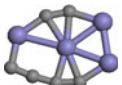, the difference in atomic coordinates obtained using two functionals did not exceed 0.05 Å. According to our previous results [17], the smaller values for $|E_b|$ which can be achieved by some modification of computational scheme are closer to the measured dissociation energies than are those obtained in the spin-unrestricted DMol calculations using 'PBE' and 'P91' functionals. Noya et al. [15] obtained the same ground geometry for FeC_4 cluster using Siesta program and 'PBE' functional; however, their $|E_b| = 23.4$ eV is noticeably less than our 'PBE' (26.4 eV) and even 'BLYP' (24.7 eV) values. The part of this difference is due to systematic overestimation of $-E_b$ obtained in DMol calculations for Fe_nC_m particles as compared with Siesta method, and another part of the difference is due to the thermal smearing which is used in the present calculations. On the other hand, Ma et al. [16] predicted the linear ground structure for FeC_4 cluster using the same DMol method and almost the same computational procedure with
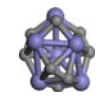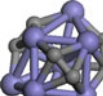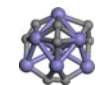
Table 1 Geometry, binding energy (eV), energy gap (eV), and ionization energies E_{i1} and E_{i2} (eV) of the ground isomers of Fe_nC_m nanoparticles (large spheres correspond to Fe atoms and small spheres correspond to C atoms)

Composition	Shape	Symmetry	Binding energy		Energy gap		E_{i1} E_{i2}	
			PBE	BLYP	PBE	BLYP	PBE	BLYP
FeC_4		C_{2V}	−26.4	−24.7	0.83	0.68	9.02	9.04
							8.92	8.79
Fe_3C_2		C_{2V}	−20.4	−19.0	0.71	0.72	6.14	6.09
							6.13	6.05
		C_S	−20.6	−18.8	0.53	0.47	6.44	6.32
							6.33	6.21
Fe_2C_4		C_S	−30.3	−28.5	0.82	0.84	7.80	7.41
							6.97	6.75
Fe_3C_3		C_S	−27.1	−25.2	0.83	0.80	7.01	6.93
							6.96	6.87
		C_1	−27.2	−25.1	0.63	0.60	7.23	6.99
							6.72	6.64
Fe_3C_4		C_{2V}	−34.9	−32.4	0.72	0.68	7.11	7.00
							6.80	6.67
Fe_4C_3		C_1	−31.7	−29.0	0.57	0.46	6.99	6.84
							6.95	6.79
Fe_3C_5		C_S	−42.1	−39.2	0.71	0.81	7.09	7.00
							6.99	6.91
Fe_4C_4		C_2	−38.8	−35.6	0.33	0.28	6.97	6.83
							6.92	6.79
Fe_4C_5		C_S	−46.3	−42.9	0.69	0.66	6.79	6.62
							6.75	6.57
Fe_5C_4		C_{2V}	−43.4	−39.6	0.27	0.30	6.35	6.19
							6.29	6.13
Fe_4C_6		C_S	−53.2	−49.6	0.29	0.38	7.04	6.88
							6.97	6.80

Table 1 continued

Composition	Shape	Symmetry	Binding energy		Energy gap		E_{i1} E_{i2}	
			PBE	BLYP	PBE	BLYP	PBE	BLYP
Fe_5C_5		C_S	−50.1	−46.1	0.07	0.06	6.26 6.23	6.12 6.09
Fe_4C_7		C_S	−60.4	−56.5	0.56	0.51	6.88 6.84	6.75 6.70
Fe_5C_6		C_S	−57.5	−52.9	0.48	0.59	6.74 6.69	6.58 6.50
		C_1	−57.1	−53.0	0.51	0.52	6.72 6.64	6.56 6.46
Fe_6C_5		C_S	−54.5	−49.5	0.39	0.51	6.36 6.26	6.09 6.08
		C_1	−54.4	−49.5	0.19	0.01	6.55 6.49	6.36 6.31
Fe_4C_8		C_S	−67.2	−63.1	0.07	0.23	7.14 7.05	6.93 6.79
Fe_5C_7		C_S	−64.5	−59.4	0.72	0.59	7.31 7.12	7.30 7.14
		C_1	−64.4	−59.7	0.35	0.60	6.58 6.53	6.65 6.46
Fe_6C_6		C_S	−61.7	−56.9	0.41	0.49	6.52 6.44	7.18 6.79
Fe_5C_8		C_S	−72.2	−67.2	0.31	0.24	6.97 6.82	6.83 6.64
Fe_6C_7		C_1	−69.3	−63.5	0.37	0.03	6.70 6.65	6.92 6.54
Fe_7C_6		C_S	−65.6	−59.9	0.35	0.04	6.40 6.35	6.20 6.14
		C_1	−65.4	−60.1	0.02	0.33	6.30 6.06	6.80 6.39

Table 1 continued

Composition	Shape	Symmetry	Binding energy		Energy gap		E_{i1} E_{i2}	
			PBE	BLYP	PBE	BLYP	PBE	BLYP
Fe_6C_8		C_1	−76.4	−70.2	0.38	0.56	6.98	6.79
							6.94	6.76
		C_1	−75.8	−70.4	0.15	0.26	6.63	6.21
							6.52	6.16
Fe_7C_7		C_1	−73.9	−67.4	0.05	0.02	7.04	6.82
							6.87	6.59
		C_1	−73.9	−67.5	0.21	0.07	6.55	6.47
							6.47	6.28
Fe_7C_8		C_1	−81.4	−74.7	0.14	0.03	7.24	7.57
							7.14	6.58

BLYP functional. We also considered a linear structure with the Fe atom at one end as a possible candidate for FeC_4 ground geometry. In agreement with the results of [16], the binding energy of our C_{2v} planar structure (Table 1) is 0.3 eV higher than that of the linear structure when the BLYP exchange–correlation potential is used. However, according to our calculations using PBE functional, the E_b of the planar structure is 0.4 eV lower than that of the linear isomer. In addition to the comparison of binding energies, the various shifts (0.1–0.3 Å) of Fe atom from equilibrium position were considered. A shift of Fe atom by 0.3 Å led to a transformation of the linear isomer into the arched chain, while the planar structure appeared to be more stable. The composition Fe_2C_4 was also investigated in [16]; unfortunately, only the high-symmetrical cyclic configurations (C_{2h}, C_{2v}, D_{2h}) were considered by the authors. Our procedure of successive addition of atoms 'one by one' allows one to obtain a wide series of high-symmetrical clusters as well as low-symmetrical ones. The comparison of E_b for several Fe_2C_4 isomers obtained using both functionals shows that C_S structure presented in Table 1 is more stable than all cyclic and linear structures considered in [16].

For some (n, m) compositions, the energetic ordering of the highest energy structures is different for 'PBE' and 'BLYP' approaches (Table 1); for Fe_3C_3, Fe_6C_5, and Fe_7C_7, the binding energy for two of the most stable conformations lies within 0.1 eV of each other, making it impossible to know which of them is the ground isomer. In these cases, both of the structures were considered as the ground geometry and were used for generating the next $Fe_{n+1}C_m$ or Fe_nC_{m+1} particles. Note that the highest point symmetry detected for the most stable isomers is C_{2V} and the most frequently obtained point group is C_S. The planar structures are typical for the ground isomers of small clusters with $n + m \leq 6$ and for some particles containing four metal atoms: Fe_4C_5, Fe_4C_6, Fe_4C_7 and Fe_4C_8. The latter particle is the largest planar ground structure obtained in our work, and we can suggest that Fe_4C_8 is the 'last' planar ground isomer among other Fe_nC_m ground geometries. However, the Fe_5C_8 and Fe_6C_8 (#2) clusters have the structures which are close to planar. Analysis of the shapes of ground isomers with planar configurations (or close to planar) shows that in addition to C_2 carbon pairs, the C_3 and C_4 carbon chains are typical for such type of geometry. In the cases of three-dimensional shape, the most common feature obtained in geometry optimization is the distorted Fe_4 quadrilateral (not planar in some configurations) centered by carbon C_2 group (Table 1). The same geometrical feature was detected for some optimized structures of $Fe_{12}C_{12}$ cluster in [8].

The energy gaps between occupied and vacant molecular states defined as the difference of energy of the highest occupied (HOMO) and the lowest unoccupied (LUMO) molecular orbitals for all investigated ground isomers are also presented in Table 1. In the majority of compositions, both functionals give the gap values of the same order of magnitude; however, for (6,5), (6,7), and (7,6) clusters, the

gaps obtained with PBE and BLYP potentials are considerably different. In some compositions, the HOMO and LUMO correspond to spin down orbitals, in the rest cases one of the orbital belongs to spin up and the other to spin down type. We do not found any ground isomer where both orbitals correspond to the spin up states. Typically, the HOMO and LUMO in investigated clusters contain 70–90% of the Fe 3d atomic orbital with admixtures of Fe4s, 4p and C2p character. In the small particles FeC_4 and Fe_3C_2, the HOMO and LUMO also contain C2s character (up to 12%). In the clusters containing greater number of atoms, the contributions of C2s orbitals in the HOMO and LUMO do not exceed 1%.

The absolute value of binding energy for Fe_nC_m gradually increases with increasing number of atoms; however, to evaluate the relative stability of nanoparticles with various sizes, it is more reasonable to compare the ground isomer binding energy per atom, $E_{nm} = |E_{gs}|/(m + n)$. The values of this specific energy (measured in eV/atom) for the investigated clusters are shown in Fig. 2. The results of 'BLYP' calculations are used in this figure; however, the trends of E_{nm} variation obtained with the use of 'PBE' functional are very similar to those shown in Fig. 2. For the presentation of E_{nm} values, we use the same style as of the map of observed $Fe_nC_m^+$ compositions from Ref. [7]; in bold, we indicate E_{nm} for the experimentally observed (5,6), (6,6), (5,7), (6,7), (7,7), (5,8), (6,8), and (7,8) compositions. As can be seen, the value of E_{nm} gradually increases with increasing number of carbon atoms 'm' (number of Fe atoms 'n' is constant) by 1.5–0.4 eV on each step for the small particles and by 0.2–0.1 eV for the particles with $n + m > 10$. On the other hand, the specific energy decreases with increasing number of iron atoms 'n' ('m' is constant) by 0.2–0.1 eV on each step for all investigated clusters with $n + m > 3$. According to these trends, the most stable particle among investigated in our work is Fe_4C_8; however, this composition was not detected in experiment
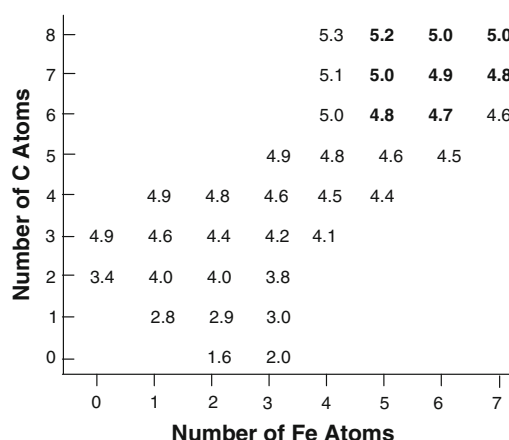
Fig. 2 The absolute values of binding energy per atom (eV/atom) for the ground isomers of neutral Fe_nC_m nanoparticles

by Pilgrim and Duncan [7]; moreover, the greater abundance of $Fe_7C_8^+$ [3] in comparison with (5,8) and (6,8) compositions is not in agreement with E_{nm} variation.

The absence of correlation between stability of neutral Fe_nC_m ground isomers and their experimental relative abundance, we could try to explain by the fact that results of Pilgrim and Duncan [7] correspond to the ionic $Fe_nC_m^+$ clusters. To verify this suggestion, we considered the configurations and stability of charged $Fe_nC_m^+$ particles. The search for ground isomers of $Fe_nC_m^+$ was undertaken using the results obtained for neutral Fe_nC_m clusters. The geometry optimization of initial structures for each (n, m) composition of neutral particles usually leads to several stable geometries, of which 5–10 have the binding energy close to that of the ground isomer. These 'more stable' neutral configurations (as well as the ground state structures) were used for the investigation of ionization process and to obtain the cationic ground isomers. Firstly, we performed the calculations of all obtained Fe_nC_m particles with fixed atomic positions and with one electron removed from the cluster. On the second step, the 'neutral' configurations were subjected to geometry optimization with one electron removed from the cluster. The ionization energy of a cluster is defined as $E_i = E_b^+ - E_b$, where E_b^+ and E_b are the binding energies of the charged and neutral particle, respectively. The ionization energies obtained on the first step (E_{i1}) include the effects of electron density relaxation which take place during ionization process, while the ionization energies obtained on the second step (E_{i2}) include the effects of electron density relaxation as well as the effects of relaxation of atomic positions. The ionization energies E_{i1} and E_{i2} of all ground isomers are summarized in Table 1. The analysis of ionization energies shows that in the majority of compositions, E_{i1} and E_{i2} are very close (the difference is less than 0.2 eV). However, in the cases of Fe_2C_4, Fe_3C_3(#2), Fe_3C_4, Fe_7C_6(#2), and Fe_7C_8 (calculations using BLYP functional), this difference is noticeably greater (from 0.3 to 1 eV). Mainly, this effect is due to the noticeable transformation of geometrical structure during ionization of the cluster; however, in the cases of Fe_3C_3(#2) and Fe_7C_8, the reordering of spin moments on metal atoms also takes place. The latter effects will be considered in next section.

The energetic ordering of ionic structures usually was not the same as for the parent neutral configurations, after analysis of the results obtained in these calculations the lowest-energy geometry was then considered as the ground state for $Fe_nC_m^+$ composition. The values of specific energy E_{nm}^+ for the ionic particles are shown in Fig. 3, as in the previous case the results of 'BLYP' calculations were presented. As can be seen from Fig. 3, the values of E_{nm}^+ considerably differ from those obtained for the corresponding neutral particles, especially for the compositions
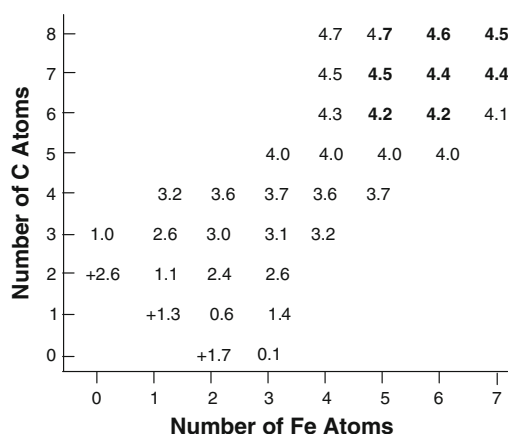
Fig. 3 The specific E_{nm}^+ energy (eV/atom) for the ground isomers of charged $Fe_nC_m^+$ nanoparticles ('+' of the values for dimers means that their binding energies are positive)

with $n + m < 8$. For Fe_2^+, FeC^+, and C_2^+ dimers, we obtained positive binding energies, this result means that such ionic species are not stable. The rest part of investigated charged clusters has negative binding energy; however, E_{nm}^+ for the particles containing 3 atoms are several times less than corresponding E_{nm} for the neutral clusters. For the ionic particles containing 4 atoms, these energies are almost two times less than corresponding 'neutral' values, and for the 5–6-atom objects, E_{nm}^+ are ~1.5 times less than those for the corresponding neutral clusters. For the ground isomers with $n + m > 7$, this energy decreases less considerably, but in all cases, the difference in specific energy for charged and neutral particles is not less than 0.4–0.5 eV/atom. The analysis of E_{nm}^+ variation shows that these values also gradually increase with increasing number of carbon atoms 'm' ('n' is constant) by at least 0.3 eV on each step for the small particles and by 0.2 eV for the particles with $n + m > 10$. However, the trends for 'horizontal' series (increasing 'n', 'm' is constant) for $Fe_nC_m^+$ clusters are noticeably different for small clusters and for those with $n + m > 7$. For the former particles E_{nm}^+ increases by 1.2–0.1 eV on each step, but for the latter compositions, E_{nm}^+ variation is very smooth, e.g., the stability of ground isomers for $Fe_nC_5^+$ ($n = 3$–6) is nearly the same. For $Fe_nC_6^+$, $Fe_nC_7^+$, and $Fe_nC_8^+$ series, E_{nm}^+ slowly decreases by 0.2 eV/atom when n increases from 4 to 8. According to these results, we can suggest that the greater abundance of $Fe_7C_8^+$ in comparison with (5,8) and (6,8) compounds is not directly connect with the stability of corresponding ground isomers.

On the other hand, according to the experimental conditions, the species with high ionization energies collect electrons from species with low ionization energies. Consequently, the cations extracted into the mass-spectrometer are likely to be those with the lowest ionization energies. It

is important to note that the values of E_i presented in Table 1 correspond to the isomers which are the ground configurations for the neutral clusters. However, as mentioned above, for each composition, the ionization process was also investigated for several 'more stable' isomers. The results of these calculations show that the ionization energies of some of the isomers are noticeably less than those presented in Table 1. For example, the lowest ionization energies for the (5,6), (5,7), (6,6), (5,8), (6,7), (6,8), (7,7), and (7,8) compositions (detected in experiment) are 6.1, 5.8, 5.8, 6.3, 6.2, 5.6, 5.8, and 6.2 eV, respectively. Figure 3 shows that the lowest E_{nm}^+ value for the clusters observed in experiment (4.2 eV/atom) was obtained for the (5,6) and (6,6) compositions and their corresponding ionization energies are 6.1 and 5.8 eV. On the other hand, there are three more stable compositions not observed in experiment (Fig. 3): Fe_4C_6 ($E_{nm}^+ = 4.3$ eV/atom), Fe_4C_7 ($E_{nm}^+ = 4.5$ eV/atom) and Fe_4C_8 ($E_{nm}^+ = 4.7$ eV/atom). According to our calculations, the lowest ionization energies obtained for these compositions are: 6.2, 6.3, and 6.7 eV, respectively. Thus, the comparison of specific and ionization energies shows that both factors can be due to the experimental cation distribution. However, this analysis cannot explain the great experimental abundance of Fe_7C_8 composition with $E_{nm}^+ = 4.5$ eV/atom and the lowest value of ionization energy $E_i = 6.2$ eV.

Another reason which could be responsible for different relative abundance is the number of stable conformations for each (n, m) composition. It is evident that all possible isomers could be found for small clusters only, for this reason in the present work, we could evaluate only the number of 'more stable' configurations for each (n, m) composition. For the most stable $Fe_4C_8^+$ composition (not observed in experiment), we obtained 15 isomers, only 3 of them had binding energies in $[E_{bg}; E_{bg} - 1$ eV$]$ interval (where E_{bg} is the energy of ground structure) and no one of them fell into $[E_{bg}; E_{bg} - 0.5$ eV$]$ range. For further comparison, we marked this result as '0/3'. For $Fe_5C_8^+$ (observed in experiment with small abundance), we obtained 5 isomers in '1 eV—limit' and 2 isomers belonging to '0.5 eV—limit'; thus, this composition can be characterized by '2/5' value. For $Fe_6C_8^+$ (also observed in experiment with small abundance), the corresponding value is also 2/5. However, for the first composition with essential abundance $Fe_7C_8^+$, we obtained 11 isomers in $[E_{bg}; E_{bg} - 1$ eV$]$ interval and 7 structures belonging to $[E_{bg}; E_{bg} - 0.5$ eV$]$ interval, i.e., the 'density of isomers' for this composition can be defined as 7/11. For the less stable compositions with seven carbon atoms, we obtained 3/6 for $Fe_4C_7^+$ (not observed in experiment), 4/6 for $Fe_5C_7^+$ (observed in experiment), 7/7 for $Fe_6C_7^+$, and 4/4 for $Fe_7C_7^+$ (both observed in experiment). For the clusters with six carbon atoms, these values are: 1/1 for $Fe_4C_6^+$ (not

observed in experiment), 6/6 and 7/9 for $Fe_5C_6{}^+$ and $Fe_6C_6{}^+$ (both observed in experiment) and 3/3 for $Fe_7C_6{}^+$ (not observed in experiment). It is evident that '1 eV' and '0.5 eV' limits used in such crude evaluation are quite arbitrary, and defined numbers of isomers are of qualitative nature. However, the analysis of stability of ground configurations and the numbers of most stable isomers allows one to conclude that the latter factor is also due to the experimental results obtained by Pilgrim and Duncan [7].

4 Effective charges and total spin densities on atoms

The most popular analyses of charge and spin density distribution based on the Mulliken or related methods depend strongly on the basis set used in the calculation and on the method of partitioning the overlap populations of each pair of atoms to the individual atoms in the pair. The more 'physical' types of population analysis use spatial integration of electron density. One of such approach was suggested by Hirshfeld [24]; in this scheme, the partition of electron density between atoms is made by the use of a 'partition function', $g_\alpha(\mathbf{r} - \mathbf{R}_\alpha)$ (α is an atom index), which is large for small $\mathbf{r} - \mathbf{R}_\alpha$ and small for large $\mathbf{r} - \mathbf{R}_\alpha$. The most popular choice for this function is $g_\alpha(\mathbf{r}) = \rho_\alpha(\mathbf{r})$, where $\mathbf{r} = |\mathbf{r}_i - \mathbf{R}_\alpha|$ and $\rho_\alpha(\mathbf{r})$ is the charge density for atom α. The drawback of this method is the dependence of Q_{eff} on the shape of the partition function. On the other hand, the most natural boundary for electron density partitioning is the locus of points of the $\rho(\mathbf{r})$ minimum. A method for the realization of this idea using numerical spatial integration incorporated in DV method was reported in Ref. [27]. Another advantage of this approach is the ability to separately integrate the spin up and spin down densities on a given atom. The sum of these values gives the effective charge (Q_{eff}) of the atom, while their difference gives the total spin density (S_{eff}) on the atom. In the previous work [17], this method was applied to the small Fe_nC_m nanoparticles, and the comparison of various schemes for the atomic effective charge calculations demonstrated that the most realistic values were obtained using the spatial numerical integration method [27]. However, in contrast to Q_{eff}, the magnetic moments on the atoms and their ordering in the small Fe_nC_m clusters were very similar when calculated using either $DMol^3$ (Hirshfeld) or DV (integration) methods [17].

The values of Q_{eff} in unit of e, where e is the electron charge, and S_{eff} in μ_B obtained for the ground isomers of all investigated Fe_nC_m ground isomers are listed in Table 2. The order of Q_{eff} and S_{eff} values corresponds to the order of atomic coordinates in Appendix; this allows one to associate of Q_{eff} and S_{eff} results with specific atoms in the structures. As can be seen, the values of Q_{eff} computed by

the DV integration scheme [27] are 2–3 times greater than those calculated by Hirshfeld procedure [24]. In the former approach, the greatest charge on the Fe atom was found to be 1.08 in the Fe_6C_8 (#1) cluster, while in the latter approach, the greatest charge on metal atom (0.4) was obtained in FeC_4. Similar results were obtained for carbon atoms, the greatest absolute value of $|Q_{eff}|$ (DMol) on C atom was found to be 0.24 in the Fe_3C_3(#2) and Fe_4C_3 clusters, the corresponding $|Q_{eff}|$ (DVM) was found to be 1.21 for the of Fe_7C_7(#1) particle (Table 2).

As mentioned above, for the small Fe_nC_m clusters, the values of S_{eff} obtained in both approaches were very similar [17], and the same results were obtained in the present calculations. For the majority of (n, m) compositions, the values of S_{eff} on Fe and C atoms computed by $DMol^3$ and DVM are in surprisingly close agreement (Table 2). The considerable disagreement was obtained only for the ground isomer of Fe_3C_4 cluster, where in the DMol calculations, S_{eff} of the two equivalent Fe atoms (2.70) is essentially greater than the total spin of these atoms obtained in DV approach (0.76). The comparison of electronic structure features of this cluster obtained in DMol and DV methods shows that the structure of Fe3d levels is considerably different in two approaches; in particular, the gap between HOMO (Fe3d spin down) and LUMO (Fe3d spin up) was found to be ~0.7 eV in DMol calculations (Table 1) and only 0.2 eV in DVM calculations. Since the $DMol^3$–GGA method provides a more accurate solution of the DFT equations than DVM–LDA, we can predict that all Fe atoms in the ground isomer of Fe_3C_4 cluster will have the high spin configuration and their total spin density will be close to 2.7.

Table 2 shows the ferromagnetic ordering (FM) of spins in the ground isomers of almost all investigated compositions. However, in some cases, the antiferromagnetic (AFM) ordering (or the ordering were the spin of at least one metal atom has an opposite direction to those of the other Fe atoms) was obtained for one of the two possible ground isomers. For Fe_3C_3(#1), Fe_5C_6(#2), Fe_6C_5(#2), Fe_5C_7(#1), and Fe_6C_8(#2) particles, the total spin densities at all metal sites have the same direction, while the second ground configurations of these compositions demonstrate the spin ordering where some magnetic moments on Fe atoms have the opposite direction. There is only one (7,6) composition for which in both possible ground conformations two opposite spin directions on metal atoms were obtained. Moreover, in the case of Fe_7C_6, we did not find isomers with FM ordering neither for the neutral nor for the charged particles, so we can conclude that FM ordering for this composition is not probable at least for the more stable isomers. Also noteworthy are the results for the greatest and smallest values of S_{Fe}, the former were found to be 3.35 (DMol) and 3.41 (DVM) in the Fe_4C_5 and Fe_4C_6

Table 2 Effective charges (e) and total spin densities (μ_B) on atoms in Fe_nC_m nanoparticles

Composition			Fe				C				
FeC$_4$	DMol	Q_{eff}	0.40				−0.03	−0.03	−0.17	−0.17	
		S_{eff}	2.27				0.04	0.04	−0.02	−0.02	
	DVM	Q_{eff}	0.94				−0.07	−0.07	−0.40	−0.40	
		S_{eff}	3.17				0.06	0.06	0.22	0.22	
Fe$_3$C$_2$ (#1)	DMol	Q_{eff}	0.12	0.11	0.11		−0.17	−0.17			
		S_{eff}	3.01	2.51	2.51		0.05	0.05			
	DVM	Q_{eff}	0.16	0.44	0.44		−0.52	−0.52			
		S_{eff}	3.16	3.19	3.19		0.06	0.06			
Fe$_3$C$_2$ (#2)	DMol	Q_{eff}	0.12	0.14	0.14		−0.23	−0.18			
		S_{eff}	2.69	2.80	2.80		−0.01	0.03			
	DVM	Q_{eff}	0.33	0.34	0.34		−0.48	−0.53			
		S_{eff}	2.91	2.90	2.90		−0.05	0.04			
Fe$_2$C$_4$	DMol	Q_{eff}	0.25	0.22			−0.02	−0.20	−0.07	−0.18	
		S_{eff}	2.82	2.93			0.07	0.07	0.06	0.14	
	DVM	Q_{eff}	0.47	0.51			−0.19	−0.28	−0.11	−0.40	
		S_{eff}	3.31	3.28			0.08	0.14	0.06	0.10	
Fe$_3$C$_3$ (#1)	DMol	Q_{eff}	0.12	0.20	0.05		−0.12	−0.18	−0.07		
		S_{eff}	2.16	2.99	3.12		−0.13	−0.15	0.03		
	DVM	Q_{eff}	0.43	0.42	0.06		−0.55	−0.34	−0.02		
		S_{eff}	2.38	2.99	3.23		−0.17	−0.18	0.04		
Fe$_3$C$_3$ (#2)	DMol	Q_{eff}	0.18	0.18	0.26		−0.24	−0.19	−0.18		
		S_{eff}	2.44	−1.67	2.93		0.02	0.10	0.01		
	DVM	Q_{eff}	0.76	0.76	0.50		−1.01	−0.47	−0.54		
		S_{eff}	2.47	−2.02	3.21		0.02	0.13	−0.06		
Fe$_3$C$_4$	DMol	Q_{eff}	0.22	0.25	0.25		−0.18	−0.18	−0.18	−0.18	
		S_{eff}	2.65	2.70	2.70		0.02	0.02	0.02	0.02	
	DVM	Q_{eff}	0.74	0.93	0.93		−0.65	−0.65	−0.65	−0.65	
		S_{eff}	2.52	0.76	0.76		0.01	0.01	0.01	0.01	
Fe$_4$C$_3$	DMol	Q_{eff}	0.16	0.20	0.17	0.10	−0.24	−0.23	−0.16		
		S_{eff}	2.58	2.88	3.14	3.07	−0.17	0.07	0.10		
	DVM	Q_{eff}	0.60	0.65	0.31	0.28	−0.88	−0.43	−0.53		
		S_{eff}	2.53	2.90	3.26	3.08	−0.25	0.10	0.12		
Fe$_3$C$_5$	DMol	Q_{eff}	0.16	0.28	0.28		−0.18	−0.18	−0.06	−0.15	−0.15
		S_{eff}	2.14	2.95	2.95		0.11	0.11	0.11	−0.19	−0.19
	DVM	Q_{eff}	0.67	0.80	0.80		−0.55	−0.55	−0.05	−0.56	−0.56
		S_{eff}	2.38	3.04	3.04		0.07	0.07	0.11	−0.15	−0.15

Table 2 continued

Composition			Fe	C
Fe$_4$C$_4$	DMol	Q_{eff}	0.17 0.17 0.22 0.22	−0.17 −0.17 −0.22 −0.22
		S_{eff}	3.03 3.03 2.97 2.97	0.09 0.09 0.13 0.13
	DVM	Q_{eff}	0.29 0.29 0.71 0.71	−0.51 −0.51 −0.49 −0.49
		S_{eff}	3.29 3.29 3.10 3.10	0.10 0.10 0.12 0.12
Fe$_4$C$_5$	DMol	Q_{eff}	0.10 0.16 0.27 0.14	−0.17 −0.19 −0.06 −0.13 −0.12
		S_{eff}	2.14 3.35 3.00 3.29	0.15 0.13 0.07 −0.08 −0.10
	DVM	Q_{eff}	0.50 0.36 0.98 0.31	−0.52 −0.59 −0.03 −0.53 −0.48
		S_{eff}	2.27 3.26 3.16 3.25	0.13 0.13 0.10 −0.09 −0.12
Fe$_5$C$_4$	DMol	Q_{eff}	0.18 0.09 0.09 0.17 0.17	−0.18 −0.18 −0.17 −0.17
		S_{eff}	2.92 3.29 3.29 3.01 3.01	0.14 0.14 0.07 0.07
	DVM	Q_{eff}	0.84 0.30 0.30 0.45 0.45	−0.56 −0.56 −0.61 −0.61
		S_{eff}	3.05 3.20 3.20 3.05 3.05	0.09 0.09 0.06 0.06
Fe$_4$C$_6$	DMol	Q_{eff}	0.15 0.19 0.27 0.18	−0.19 −0.04 −0.03 −0.16 −0.16 −0.20
		S_{eff}	2.54 3.28 2.97 3.25	0.11 0.03 0.09 0.12 0.11 −0.01
	DVM	Q_{eff}	0.41 0.43 0.95 0.40	−0.58 −0.02 −0.14 −0.09 −0.51 −0.41
		S_{eff}	2.82 3.38 3.28 3.41	0.13 0.04 0.11 0.02 0.11 0.06
Fe$_5$C$_5$	DMol	Q_{eff}	0.09 0.14 0.25 0.12 0.12	−0.17 −0.18 −0.16 −0.05 −0.16
		S_{eff}	2.42 3.10 3.04 3.17 3.17	0.15 0.12 0.03 0.11 0.05
	DVM	Q_{eff}	0.41 0.30 0.98 0.31 0.31	−0.54 −0.58 −0.48 −0.09 −0.62
		S_{eff}	2.10 2.94 3.25 3.04 3.04	0.13 0.11 −0.02 0.12 −0.04
Fe$_4$C$_7$	DMol	Q_{eff}	0.17 0.26 0.29 0.26	−0.18 −0.17 −0.03 −0.21 −0.15 −0.04 −0.21
		S_{eff}	2.46 2.14 3.14 2.11	0.04 0.10 0.01 0.07 0.03 0.09 0.03
	DVM	Q_{eff}	0.67 1.00 0.89 1.01	−0.57 −0.55 −0.09 −0.56 −0.40 −0.21 −1.19
		S_{eff}	2.57 2.02 3.32 2.09	0.05 0.06 0.02 0.03 0.05 0.08 −0.21
Fe$_5$C$_6$ (#1)	DMol	Q_{eff}	0.20 0.22 0.18 0.26 0.22	−0.22 −0.15 −0.16 −0.16 −0.17 −0.17
		S_{eff}	2.92 2.97 2.91 2.83 2.92	0.16 0.11 0.02 0.02 0.05 0.05
	DVM	Q_{eff}	0.67 0.70 0.43 0.48 0.67	−0.50 −0.48 −0.58 −0.63 −0.58 −0.63
		S_{eff}	2.65 2.81 2.84 2.94 2.65	0.13 0.08 −0.04 0.02 −0.04 0.02
Fe$_5$C$_6$ (#2)	DMol	Q_{eff}	0.13 0.13 0.14 0.16 0.13	−0.17 −0.18 −0.04 −0.15 −0.18 −0.04
		S_{eff}	2.80 3.06 3.12 2.83 3.11	0.11 0.11 0.05 0.09 0.11 0.10
	DVM	Q_{eff}	0.32 0.41 0.43 0.48 0.97	−0.51 −0.63 −0.06 −0.54 −0.63 −0.12
		S_{eff}	2.71 3.01 3.04 2.94 3.38	0.09 0.10 0.04 0.09 0.10 0.11
Fe$_6$C$_5$ (#1)	DMol	Q_{eff}	0.16 0.16 0.16 0.14	−0.23 −0.16 −0.16 −0.18
		S_{eff}	2.73 2.20 2.83 −2.38	0.05 −0.01 −0.01 0.05
	DVM	Q_{eff}	0.69 0.56 0.48 0.66	−1.15 −0.60 −0.60 −0.59
		S_{eff}	2.61 2.65 2.94 −2.61	0.05 −0.04 −0.04 0.05

Table 2 continued

Composition			Fe							C							
Fe₆C₅ (#2)	DMol	Q_{eff}	0.17	0.13	0.19	0.18	0.11	0.12		−0.16	−0.15	−0.18	−0.19	−0.22			
		S_{eff}	2.24	2.67	2.40	2.94	3.25	3.19		0.10	0.10	0.15	0.10	−0.22			
	DVM	Q_{eff}	0.82	0.35	1.04	0.41	0.17	0.41		−0.66	−0.51	−0.54	−0.54	−0.95			
		S_{eff}	2.52	2.68	2.34	2.96	3.24	3.26		0.11	0.08	0.14	0.09	−0.22			
Fe₄C₈	DMol	Q_{eff}	0.24	0.29	0.29	0.29				−0.17	−0.03	−0.17	−0.14	−0.21	−0.04	−0.17	−0.16
		S_{eff}	2.96	3.21	2.66	2.83				0.10	0.05	0.10	0.10	0.07	0.10	0.12	0.12
	DVM	Q_{eff}	0.63	0.96	1.00	0.96				−0.61	−0.15	−0.53	−0.38	−0.38	−0.18	−0.50	−0.56
		S_{eff}	3.15	3.40	3.20	3.16				0.10	0.06	0.10	0.08	0.08	0.14	0.14	0.13
Fe₅C₇ (#1)	DMol	Q_{eff}	0.23	0.23	0.21	0.23	0.24			−0.21	−0.13	−0.15	−0.14	−0.17	−0.17	−0.18	
		S_{eff}	2.38	2.38	2.53	3.13	3.00			0.21	0.14	0.12	−0.06	0.10	0.11	−0.29	
	DVM	Q_{eff}	1.01	1.01	0.77	0.68	0.87			−0.46	−0.54	−0.55	−0.50	−0.53	−0.63	−0.98	
		S_{eff}	2.33	2.33	2.50	3.09	3.09			0.19	0.11	0.13	−0.01	0.10	0.10	−0.28	
Fe₅C₇ (#2)	DMol	Q_{eff}	0.21	0.08	0.21	0.26	0.24			−0.14	−0.05	−0.19	−0.05	−0.17	−0.17	−0.14	
		S_{eff}	2.84	1.94	2.91	−2.86	−2.86			−0.06	−0.01	0.12	−0.01	0.04	0.10	−0.11	
	DVM	Q_{eff}	0.75	0.31	0.62	0.97	0.66			−0.50	−0.02	−0.57	−0.02	−0.64	−0.53	−0.49	
		S_{eff}	2.69	1.70	2.83	−3.11	3.00			−0.01	−0.01	0.08	−0.01	−0.02	0.06	−0.09	
Fe₆C₆	DMol	Q_{eff}	0.18	0.17	0.16	0.20	0.20	0.16		−0.14	−0.18	−0.18	−0.18	−0.22	−0.14		
		S_{eff}	2.93	2.94	2.92	2.88	2.88	2.92		0.06	0.09	0.09	0.09	0.10	0.06		
	DVM	Q_{eff}	0.75	0.36	0.47	0.50	0.72	0.50		−0.67	−0.57	−0.59	−0.55	−0.55	−0.67		
		S_{eff}	2.90	2.95	2.96	2.95	2.84	2.92		0.03	0.06	0.06	0.05	0.05	0.03		
Fe₅C₈	DMol	Q_{eff}	0.21	0.11	0.19	0.29	0.18			−0.17	−0.18	−0.16	−0.13	−0.03	−0.03	−0.15	−0.15
		S_{eff}	2.54	2.40	2.40	3.12	2.02			0.06	0.11	0.06	0.04	0.04	0.03	0.04	0.04
	DVM	Q_{eff}	0.79	0.28	0.28	1.01	1.06			−0.57	−0.54	−0.54	−0.53	−0.13	−0.13	−0.44	−0.44
		S_{eff}	2.59	2.46	2.46	3.14	1.63			0.01	0.08	0.08	0.03	0.03	0.03	0.06	0.06
Fe₆C₇	DMol	Q_{eff}	0.20	0.18	0.19	0.22	0.18	0.18		−0.18	−0.15	−0.17	−0.16	−0.16	−0.19	−0.19	
		S_{eff}	2.97	2.89	2.50	2.50	2.02	2.02		0.10	0.08	0.07	0.11	0.10	0.11	−0.25	
	DVM	Q_{eff}	0.67	0.77	0.46	0.81	1.00	1.06		−0.65	−0.56	−0.65	−0.61	−0.65	−0.64	−1.01	
		S_{eff}	2.95	2.93	2.99	2.67	2.32	1.63		0.08	0.06	0.07	0.05	0.08	0.07	−0.26	
Fe₇C₆ (#1)	DMol	Q_{eff}	0.14	0.17	0.12	0.19	0.12	0.19	0.19	−0.16	−0.18	−0.18	−0.16	−0.11	−0.11		
		S_{eff}	2.87	2.76	2.78	−2.37	2.78	−2.37	−2.37	0.04	0.11	0.11	0.04	−0.04	−0.04		
	DVM	Q_{eff}	0.61	0.47	0.37	0.79	0.37	0.79	0.79	−0.53	−0.61	−0.61	−0.60	−0.66	−0.66		
		S_{eff}	2.55	2.66	2.56	−2.65	2.56	−2.65	−2.65	−0.02	0.05	0.05	0.03	−0.03	−0.03		
Fe₇C₆ (#2)	DMol	Q_{eff}	0.10	0.13	0.13	0.14	0.20	0.18	0.20	−0.16	−0.17	−0.16	−0.18	−0.16	−0.16		
		S_{eff}	3.07	2.57	2.76	2.50	−2.78	2.50	−2.70	0.04	0.05	−0.01	0.02	−0.04	−0.04		
	DVM	Q_{eff}	0.28	0.24	0.37	0.48	0.79	0.81	0.78	−0.56	−0.51	−0.58	−0.65	−0.58	−0.58		
		S_{eff}	3.00	2.40	2.71	2.55	−2.89	2.50	−2.82	0.03	0.03	−0.03	0.02	−0.06	−0.06		

Table 2 continued

Composition	Method		Fe							C							
Fe$_6$C$_8$ (#1)	DMol	Q_{eff}	0.20	0.19	0.22	0.22	0.20	0.19		-0.14	-0.14	-0.14	-0.14	-0.14	-0.14	-0.19	-0.19
		S_{eff}	2.02	1.74	2.26	-2.27	-2.03	-1.74		0.04	-0.02	0.02	0.02	-0.03	-0.04	0.26	-0.26
	DVM	Q_{eff}	1.03	1.05	0.85	0.84	0.98	1.08		-0.67	-0.61	-0.63	-0.64	-0.61	-0.63	-1.02	-1.02
		S_{eff}	2.06	1.10	2.40	-2.41	-2.08	-1.11		0.01	-0.02	0.02	0.01	-0.01	-0.01	0.24	-0.24
Fe$_6$C$_8$ (#2)	DMol	Q_{eff}	0.15	0.13	0.09	0.27	0.24	0.22		-0.17	-0.18	-0.17	-0.16	-0.06	-0.04	-0.16	-0.16
		S_{eff}	2.65	2.65	2.61	3.07	2.98	3.04		0.06	0.08	0.13	0.05	0.06	0.06	0.02	0.06
	DVM	Q_{eff}	0.64	0.14	0.03	1.03	0.98	0.33		-0.58	-0.45	-0.43	-0.52	-0.07	-0.08	-0.52	-0.48
		S_{eff}	2.42	2.53	2.28	3.16	3.13	3.15		0.04	0.06	0.08	0.04	0.05	0.05	0.00	0.06
Fe$_7$C$_7$ (#1)	DMol	Q_{eff}	0.16	0.20	0.19	0.16	0.19	0.16	0.15	-0.17	-0.16	-0.18	-0.17	-0.16	-0.17	-0.20	
		S_{eff}	2.84	2.94	2.91	2.67	2.44	2.50	2.49	0.05	0.07	0.07	0.11	0.09	0.10	-0.18	
	DVM	Q_{eff}	0.42	0.84	0.58	0.38	1.01	0.70	0.80	-0.56	-0.51	-0.66	-0.59	-0.54	-0.66	-1.21	
		S_{eff}	2.78	2.98	2.91	2.57	2.48	2.63	2.56	0.07	0.08	0.06	0.10	0.07	0.10	-0.16	
Fe$_7$C$_7$ (#2)	DMol	Q_{eff}	0.14	0.17	0.18	0.19	0.18	0.18	0.15	-0.16	-0.16	-0.16	-0.17	-0.18	-0.16	-0.20	
		S_{eff}	2.47	2.92	2.64	2.80	2.91	2.96	2.66	0.10	0.09	0.04	0.06	0.12	0.10	-0.16	
	DVM	Q_{eff}	0.77	0.16	0.88	0.59	0.77	0.68	0.79	-0.63	-0.60	-0.51	-0.53	-0.61	-0.58	-1.18	
		S_{eff}	2.46	2.85	2.62	2.73	2.93	2.96	2.69	0.10	0.08	0.04	0.05	0.10	0.07	-0.16	
Fe$_7$C$_8$	DMol	Q_{eff}	0.17	0.21	0.17	0.17	0.23	0.17	0.22	-0.17	-0.17	-0.18	-0.17	-0.15	-0.17	-0.15	-0.18
		S_{eff}	2.94	3.02	2.94	2.97	3.10	2.95	3.02	0.09	0.09	0.12	0.14	0.12	0.12	0.12	0.14
	DVM	Q_{eff}	0.59	0.86	0.47	0.01	1.02	0.50	0.88	-0.54	-0.55	-0.62	-0.54	-0.50	-0.58	-0.51	-0.49
		S_{eff}	2.86	3.02	2.84	2.95	2.98	2.84	3.02	0.09	0.09	0.08	0.13	0.09	0.08	0.09	0.12
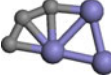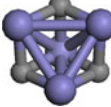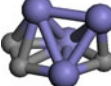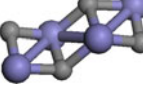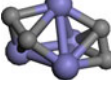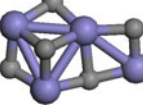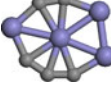
clusters, respectively (both have FM ordering), while the latter value 1.67 (DMol) and 1.10 (DVM) were obtained for the clusters Fe_3C_3 and Fe_6C_8(#1), respectively (both have AFM ordering).

In contrast to the results obtained for the neutral Fe_nC_m clusters, FM ordering in the ground isomers of charged $Fe_nC_m^+$ particles is not so preferable. Our calculations of two types of ionization show that the transformation of FM ordering to AFM one is not a simple process. In the cases of Fe_2C_4, Fe_4C_8, Fe_5C_7(#1), Fe_6C_6, Fe_5C_8, Fe_6C_7, Fe_7C_7(#1), and Fe_7C_8, the FM ordering transforms to the AFM type during simple ionization (without relaxation of atomic position) and the resulting ordering do not change during geometry optimization. For almost all compositions mentioned above, with the exception of Fe_7C_7(#1), one electron is removed from the HOMO corresponding to spin down states, but during self-consistency, the number of spin down orbitals in valence band increases. As a result, the spin moments on one or two metal atoms change their direction. In the case of Fe_4C_6, the FM ordering remains during simple ionization; however, the direction of spin moment on one Fe atom changes during relaxation of

atomic positions. It is interesting to note that in the cases of Fe_3C_3(#2) and Fe_6C_5(#1), we obtained the transformation of initial AFM ordering to FM type during 'simple' ionization; however, the ionization with geometry optimization returned the spin moments on metal atoms to the initial orientations. In all other cases, the initial AFM ordering obtained for the neutral particles did not change for the corresponding ionic clusters. On the other hand, the values of S_{Fe} for the charged clusters were obtained in the same limits as for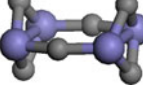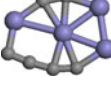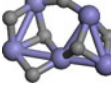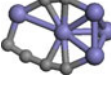 the neutral species; the greatest and smallest total spin densities at the metal atoms of $Fe_nC_m^+$ were found to be 3.4 ($Fe_5C_4^+$, FM ordering) and 1.7 ($Fe_6C_8^+$, AFM ordering).

Finally, we compared the stabilities of Fe_nC_m nanoparticles generated by two ways. The construction of Fe–C clusters by addition of atoms 'one by one' used in the present work corresponds to experimental technology of laser vaporization of Fe metal and cooling in acetylene; however, Fe–C clusters can also be produced by grinding of solid-phase carbides. For the comparison of two types of clusters, we considered the small fragments of the real crystal lattice of the most stable solid-phase carbide Fe_3C

Table 3 Comparison of the values of binding energies (eV) of the fragments of Fe_3C crystal lattice and ground isomers of Fe_nC_m nanoparticles of the same composition

Composition	Fragments of Fe_3C crystal lattice		Nanoparticles	
	Shape	E_b	Shape	E_b
Fe_3C_2		−18.5		−19.0
Fe_3C_3		−22.2		−25.2
Fe_4C_3		−28.1		−29.0
Fe_4C_4		−33.3		−35.6
Fe_4C_5		−39.1		−42.9
Fe_4C_6		−44.1		−49.6
Fe_5C_6		−48.1		−53.0

(cementite). It is evident that the stoichiometry of crystal fragments containing hundreds or thousands atoms will be close to (3,1); however, the small Fe_nC_m fragments of crystal lattice could be of various compositions. We considered seven types of crystal fragments with atomic positions corresponding to cementite lattice parameters reported in Ref. [28]. These initial structures were subjected to geometry optimization, leading to the new equilibrium geometries corresponding to the isolated clusters. In Table 3, we present the results of crystal fragments calculations, which are compared with the results obtained for corresponding Fe_nC_m clusters generated according to 'binomial' scheme. As can be seen, the absolute values of E_b of all optimized crystal fragments of either compact three-dimensional type or 'chain-type' are noticeably less than the energies obtained for corresponding nanoparticles. The comparison of these values shows that in general, the difference in stability increases with increasing number of atoms from 0.5 eV (Fe_3C_2) to 5.5 eV (Fe_4C_6).

5 Conclusions

Our investigations of Fe_nC_m nanoparticles containing 5–15 atoms do not confirm the earlier results [8] that the crystal lattice fragments of iron carbides can be the better starting point to achieve the most stable geometry of isolated clusters. Moreover, we can suppose that the construction of binary Me_nC_m particles by addition of atoms 'one by one' (corresponding to vaporization–cooling technologies) leads to more stable objects for the wide range of metcars.

The analysis of spin moments ordering shows that in the majority of ground isomers of neutral Fe_nC_m clusters investigated in the present work, the FM ordering is preferable. On the other hand, our calculations of the similar Fe–O species which are in progress now show that FM ordering is not realized in almost all ground isomers and is rarely obtained for the more stable structures of Fe_nO_m nanoparticles. Therefore, we can conclude that the binary Fe–C clusters can serve as a perspective source to obtain the molecular objects with high magnetic moments.

Appendix

See Table 4.

Table 4 Atomic coordinates (Å) in the ground isomers of Fe_nC_m nanoparticles obtained using BLYP functional

Composition	Fe			C		
FeC₄	0.0	0.0	1.179	0.692	0.0	−0.689
				−0.692	0.0	−0.689
				1.719	0.0	0.100
				−1.719	0.0	0.100
Fe₃C₂ (#1)	0.0	0.0	−1.184	−0.649	0.0	0.769
	−2.213	0.0	−0.177	0.649	0.0	0.769
	2.213	0.0	−0.177			
Fe₃C₂ (#2)	1.528	0.645	0.0	−0.918	−0.983	0.0
	−0.513	0.609	1.156	0.415	−0.879	0.0
	−0.513	0.609	−1.156			
Fe₂C₄	−0.159	−1.306	0.0	0.014	0.770	0.0
	2.269	−0.403	0.0	−2.073	−0.618	0.0
				−1.312	0.423	0.0
				1.260	1.134	0.0
Fe₃C₃ (#1)	−0.164	−0.845	0.0	−0.135	1.149	0.0
	1.696	0.853	0.0	−2.087	−0.403	0.0
	2.106	−1.486	0.0	−1.415	0.732	0.0
Fe₃C₃ (#2)	−0.497	−1.338	−0.316	1.267	−1.227	−0.275
	1.317	0.504	−0.230	−0.388	1.394	−0.299
	−0.401	0.251	1.469	−1.298	0.417	−0.349
Fe₃C₄	0.0	−1.743	−0.386	1.530	0.658	−0.108
	0.0	−1.743	−0.386	1.530	−0.658	−0.108

Table 4 continued

Composition	Fe			C		
	0.0	0.0	1.203	−1.530	−0.658	−0.108
				−1.530	0.658	−0.108
Fe$_4$C$_3$	−0.864	−0.957	−0.934	0.534	−1.762	−0.059
	0.899	−0.036	0.638	−0.180	1.657	0.272
	−1.352	0.238	1.306	−0.694	0.932	−0.685
	−0.843	−2.073	1.192			
Fe$_3$C$_5$	−0.006	0.858	0.0	1.813	−0.048	0.645
	0.420	−0.364	−2.001	1.813	−0.048	−0.645
	0.420	−0.364	2.001	−1.809	−0.070	0.0
				−1.325	0.019	1.250
				−1.325	0.019	−1.250
Fe$_4$C$_4$	0.939	−0.677	−1.389	1.334	−0.951	0.729
	−0.939	0.677	−1.389	−1.334	−0.951	0.729
	−0.897	−0.941	0.509	−0.788	1.994	0.151
	0.897	0.941	0.509	0.788	−1.994	0.151
Fe$_4$C$_5$	0.069	0.009	0.0	−0.994	1.851	0.0
	−2.414	0.565	0.0	0.279	2.069	0.0
	2.100	1.407	0.0	−0.558	−1.903	0.0
	2.407	−0.938	0.0	0.767	−1.914	0.0
				−1.656	−1.147	0.0
Fe$_5$C$_4$	0.0	0.0	−2.244	0.0	1.939	0.149
	0.0	−1.219	1.977	0.0	−1.939	0.149
	0.0	1.219	1.977	0.0	−1.556	−1.095
	1.153	0.0	0.091	0.0	1.556	−1.095
	−1.153	0.0	0.091			
Fe$_4$C$_6$	0.401	0.168	0.0	−0.754	2.968	0.0
	−2.296	0.816	0.0	0.503	2.244	0.0
	2.347	1.685	0.0	−0.108	−1.869	0.0
	2.749	−0.667	0.0	1.175	−1.782	0.0
				−2.604	−1.041	0.0
				−1.412	−1.523	0.0
Fe$_5$C$_5$	−0.099	0.131	0.0	−1.164	1.942	0.0
	−2.601	0.672	0.0	0.108	2.192	0.0
	1.918	1.441	0.0	−0.752	−1.779	0.0
	1.924	−0.840	1.145	0.607	−1.836	0.0
	1.924	−0.840	−1.145	−1.866	−1.083	0.0
Fe$_4$C$_7$	0.502	0.227	0.0	−0.950	1.819	0.0
	−2.468	0.637	0.0	0.229	2.329	0.0
	2.087	2.235	0.0	−0.453	−1.788	0.0
	2.573	−1.263	0.0	0.821	−1.887	0.0
				−3.005	−1.208	0.0
				−1.794	−1.607	0.0
				2.460	0.506	0.0
Fe$_5$C$_6$ (#1)	−1.260	0.881	1.296	−2.753	0.358	0.0
	−1.260	0.881	−1.296	−2.084	−0.751	0.0
	0.825	1.186	0.0	0.470	1.179	1.867
	−0.119	−1.072	0.0	0.470	1.179	−1.867
	2.583	−1.018	0.0	1.565	−0.412	−1.492

Table 4 continued

Composition	Fe			C		
				1.565	−0.412	−1.492
Fe$_5$C$_6$ (#2)	0.219	0.042	−0.041	−0.945	1.822	−0.177
	−2.570	0.767	−0.175	0.307	2.118	−0.070
	2.145	1.552	0.173	−0.594	−1.838	0.617
	2.369	−0.889	0.740	0.676	−1.847	0.801
	2.344	−0.122	−1.434	−3.055	−1.058	0.171
				−1.897	−1.547	0.393
Fe$_6$C$_5$ (#1)	1.191	1.703	0.0	0.324	−1.785	0.0
	−1.135	0.875	0.0	0.186	1.215	1.595
	1.367	−0.483	1.125	0.186	1.215	−1.595
	1.367	−0.483	−1.125	−0.700	0.301	−1.986
	−1.043	−1.430	−1.243	−0.700	0.301	1.986
	−1.043	−1.430	1.243			
Fe$_6$C$_5$ (#2)	1.561	−0.446	−1.118	1.600	0.220	0.947
	−1.006	−0.606	−1.007	−1.593	0.745	0.714
	0.179	1.366	0.086	−2.240	−0.392	0.776
	−0.244	−0.714	1.468	1.771	−1.086	0.869
	0.569	−2.443	−0.083	0.276	0.683	−1.638
	−1.873	−2.328	0.490			
Fe$_4$C$_8$	0.563	0.234	0.0	−0.198	2.261	0.0
	−2.830	0.461	0.0	−0.724	−1.867	0.0
	1.571	2.844	0.0	0.541	−1.978	0.0
	2.400	−1.775	0.0	−3.300	−1.407	0.0
				−2.066	−1.726	0.0
				2.789	0.028	0.0
				2.558	1.300	0.0
				−1.305	1.626	0.0
Fe$_5$C$_7$ (#1)	−1.193	0.869	1.225	−2.718	0.132	0.0
	−1.193	0.869	−1.225	−1.995	−0.938	0.0
	1.114	0.939	0.0	0.430	−0.044	1.910
	−0.036	−1.238	0.0	0.430	−0.044	−1.910
	2.558	−1.248	0.0	1.512	−0.654	−1.525
				1.512	−0.654	1.525
				−0.421	2.010	0.0
Fe$_5$C$_7$ (#2)	−1.064	1.188	1.671	−2.277	0.041	0.773
	−0.597	−0.318	−0.252	−2.523	−0.880	−0.156
	0.935	1.552	0.016	0.808	1.362	2.089
	−0.483	−2.313	−1.965	1.137	0.215	−1.389
	1.789	−0.786	0.384	0.988	−1.056	−1.665
				1.803	0.608	1.732
				−2.016	−1.614	−1.139
Fe$_6$C$_6$	1.177	2.060	0.0	0.529	−1.930	0.0
	−0.956	0.961	0.0	0.353	1.559	1.695
	1.210	−0.356	1.159	0.353	1.559	−1.695
	1.210	−0.356	−1.159	−0.491	0.624	−2.064
	−1.105	−1.146	−1.428	−0.491	0.624	2.064
	−1.105	−1.146	1.428	−0.684	−2.452	0.0
Fe$_5$C$_8$	2.235	0.067	0.0	1.989	0.018	1.916

Table 4 continued

Composition	Fe			C		
	0.116	0.189	1.196	1.989	0.018	−1.916
	0.116	0.189	−1.196	1.192	−0.061	−2.938
	−0.654	−0.179	−3.512	1.192	−0.061	2.938
	−0.654	−0.179	3.512	−1.963	0.026	0.678
				−1.963	0.026	−0.678
				−1.797	−0.027	−1.958
				−1.797	−0.027	1.958
Fe$_6$C$_7$	−1.251	1.261	1.170	−2.277	−0.053	−0.200
	−1.279	0.979	−1.458	−2.025	−0.607	0.936
	0.869	1.178	0.057	0.437	0.981	2.155
	−0.477	−1.344	−0.643	0.475	0.257	−1.858
	1.843	−1.121	0.509	1.464	−0.377	−1.268
	−0.374	−1.102	1.911	1.473	0.221	1.891
				0.475	−2.238	0.750
Fe$_7$C$_6$ (#1)	0.801	2.077	0.0	−0.164	1.522	1.631
	−1.364	0.721	0.0	−0.164	1.522	−1.631
	1.104	−0.203	1.156	−0.803	0.443	−2.020
	1.104	−0.203	−1.156	−0.803	0.443	2.020
	−1.220	−1.405	−1.474	−0.648	−2.579	0.0
	−1.220	−1.405	1.474	0.423	−1.800	0.0
	2.952	0.866	0.0			
Fe$_7$C$_6$ (#2)	1.853	1.642	−0.350	−0.229	1.073	2.536
	−0.415	1.097	0.362	0.362	1.426	−1.640
	1.142	−0.391	1.420	−0.706	0.685	−1.803
	0.914	−0.532	−1.053	−1.103	0.186	2.161
	−1.576	−1.033	−1.472	−0.310	−2.219	−0.606
	−1.345	−1.368	1.048	0.517	−2.011	0.411
	1.414	1.944	1.985			
Fe$_6$C$_8$ (#1)	−1.169	1.429	1.219	−2.145	−0.001	−0.233
	−1.128	1.177	−1.378	−1.926	−0.543	0.936
	1.059	1.309	0.015	0.452	0.869	2.127
	−0.475	−1.354	−0.600	0.451	0.144	−1.779
	−0.351	−1.099	1.925	1.460	−0.418	−1.163
	1.853	−1.249	0.536	1.505	0.163	1.811
				0.431	−2.297	0.786
				−0.514	2.370	−0.203
Fe$_6$C$_8$ (#2)	2.392	0.004	−0.074	1.960	0.088	1.830
	−0.021	−0.227	1.116	2.084	−0.050	−1.982
	0.259	0.603	−1.231	1.258	−0.075	−2.978
	−0.621	−0.189	−3.399	1.136	0.030	2.852
	−0.655	−0.015	3.505	−2.105	−0.043	0.802
	1.225	1.804	0.814	−1.810	0.075	−0.521
				−1.667	0.094	−1.813
				−1.936	−0.099	2.080
Fe$_7$C$_7$ (#1)	−1.325	0.492	1.165	−2.443	0.117	−0.637
	−1.109	1.221	−1.491	−2.639	−0.960	0.079
	0.905	1.100	0.098	0.404	0.756	2.088
	−0.519	−1.055	−0.646	0.627	0.425	−1.876

Table 4 continued

Composition	Fe			C		
	1.690	−1.338	0.396	1.488	−0.394	−1.323
	0.066	−1.298	2.354	1.522	0.077	1.839
	−1.755	−2.266	1.143	0.090	−2.376	0.811
Fe₇C₇ (#2)	1.827	2.048	−0.181	−0.403	1.070	2.621
	−0.636	1.035	0.347	0.556	1.551	−1.489
	0.851	−0.601	1.915	−0.368	0.694	−1.836
	1.081	−0.412	−0.515	−1.273	0.182	2.219
	−1.171	−1.007	−1.521	−0.202	−2.245	−0.412
	−1.514	−1.250	0.937	0.427	−2.150	0.740
	1.251	1.905	2.172	2.089	0.680	1.004
Fe₇C₈	−1.422	0.586	1.242	−2.511	0.379	−0.630
	−1.109	1.236	−1.612	−2.851	−0.622	0.130
	0.801	0.997	0.106	0.348	0.658	2.154
	−0.587	−1.037	−0.498	0.632	0.439	−1.933
	1.951	−1.296	0.320	1.541	−0.305	−1.372
	−0.042	−1.428	1.946	1.484	0.048	1.884
	−2.312	−2.244	0.989	0.668	−2.816	0.536
				−0.588	−3.093	0.738

References

1. Guo BC, Kerns KP, Castleman AW (1992) Science 255:1411
2. Redondo P, Barrientos C, Largo A (2005) J Phys Chem A 109:8594
3. Redondo P, Barrientos C, Largo A (2008) Int J Quant Chem 108:1684
4. Froudakis GE, Muhlhauser M, Andriotis AN, Menon M (2001) Phys Rev B 64:241401R
5. Longo RC, Gallego LJ (2003) J Chem Phys 118:10349
6. Toth LE (1971) Transition metal carbides and nitrides. Academic Press, N.Y.
7. Pilgrim JS, Duncan MA (1993) J Am Chem Soc 115:6958
8. Harris H, Dance I (2007) Polyhedron 26:250
9. Wang LS (1996) Surf Rev Lett 3:423
10. Nash BK, Rao BK, Jena P (1996) J Chem Phys 105:11020
11. Cao Z (1996) J Mol Struct 365:211
12. Sosa R, Gardiol P, Beltrame G (1997) Int J Quantum Chem 65:919
13. Arbuznikov AV, Hendrickx M, Vanquickenborne LG (1999) Chem Phys Lett 310:515
14. Gutsev GL, Bauschlichter CW Jr (2003) Chem Phys 291:27
15. Noya EG, Longo RC, Gallego LJ (2003) J Chem Phys 119:11130
16. Ma Q-M, Xie Z, Wang J, Liu Y, Li Y-C (2007) Phys Rev B 76:035412
17. Ryzhkov MV, Ivanovskii AL, Delley B (2005) Chem Phys Lett 404:400
18. Ryzhkov MV, Ivanovskii AL, Delley B (2008) Theor Chem Acc 119:313
19. Dmol3 β version, Molecular Simulations, San Diego (1997)
20. Perdew JP, Burke K, Ernzerhof M (1996) Phys Rev Lett 77:3865
21. Becke AD (1988) J Chem Phys 88:2547
22. Lee C, Yang W, Parr RG (1988) Phys Rev B 37:785
23. Mulliken RS (1955) J Chem Phys 23:1833
24. Hirshfeld FL (1977) Theor Chim Acta 44:129
25. Baerends EJ, Ellis DE, Ros P (1973) Chem Phys 2:41
26. Press MR, Ellis DE (1987) Phys Rev B 35:4438
27. Ryzhkov MV (1998) J Struct Khimii (Russia) 39:1134
28. Fasiska EJ, Jeffrey GA (1965) Acta Cryst 19:463